Preclinical Evaluation and Pilot Clinical Study of Al^{18}F-PSMA-BCH for Prostate Cancer PET Imaging

Teli Liu*[1], Chen Liu*[1], Xiaoxia Xu[1], Fei Liu[1], Xiaoyi Guo[1], Nan Li[1], Xuejuan Wang[1], Jianhua Yang[1], Xing Yang[2], Hua Zhu[1], and Zhi Yang[1]

[1]*Key Laboratory of Carcinogenesis and Translational Research (Beijing Ministry of Education), Department of Nuclear Medicine, Peking University Cancer Hospital and Institute, Beijing, China; and* [2]*Department of Nuclear Medicine, Peking University First Hospital, Beijing, China*

Prostate-specific membrane antigen (PSMA)–targeted radioligands have played an important role in the diagnosis of prostate cancer. In this study, we developed an Al^{18}F-labeled radiotracer and evaluated its potential for prostate cancer imaging. **Methods:** Al^{18}F-PSMA-BCH (BCH is Beijing Cancer Hospital) was efficiently prepared manually. The binding affinity to PSMA was evaluated in vitro using the 22Rv1 (PSMA-positive) cell line. Small-animal PET imaging, biodistribution studies of Al^{18}F-PSMA-BCH in mice bearing 22Rv1 and PC-3 (PSMA-negative) xenografted tumors, and a comparison with ^{68}Ga-PSMA-617 in mice bearing LNCaP tumors were performed. PET/CT imaging was performed on 11 newly diagnosed prostate cancer patients at 1 and 2 h after injection. Biodistribution and preliminary efficacy were evaluated, and radiation dosimetry was estimated using OLINDA/EXM 2.0 software. **Results:** Al^{18}F-PSMA-BCH was prepared within 30 min and was found to bind to PSMA with a dissociation constant of 2.90 ± 0.83 nM. Small-animal PET imaging of Al^{18}F-PSMA-BCH could clearly differentiate 22Rv1 tumors from PC-3 tumors, as confirmed by ex vivo biodistribution data (7.87% ± 2.37% and 0.54% ± 0.22% injected dose/g at 1 h in 22Rv1 and PC-3 tumors, respectively). The uptake of Al^{18}F-PSMA-BCH in 22Rv1 tumors could be substantially blocked by excess ZJ-43, a PSMA inhibitor. High-level accumulation of Al^{18}F-PSMA-BCH was observed in PSMA-expressing organs, with increased uptake at later time points. Thirty-seven tumor lesions were detected in 11 patients, and the SUV_{max} in 27 lesions increased between 1 and 2 h after injection (10.60 vs. 14.11). The SUV_{max} in primary lesions in patients with high-risk prostate cancer was higher than that in patients with intermediate-risk prostate cancer. The kidneys received the highest estimated dose, 0.135 mGy/MBq, and the effective dose was 0.016 mGy/MBq. **Conclusion:** Al^{18}F-PSMA-BCH was conveniently prepared with a reasonable yield within 30 min and showed a promising imaging capability for prostate cancer with reasonable radiation exposure. Al^{18}F-PSMA-BCH can be used for prostate cancer imaging as a novel ^{18}F PET radiotracer.

Key Words: Al^{18}F; PSMA; prostate cancer; PET imaging; clinical study

J Nucl Med 2019; 60:1284–1292
DOI: 10.2967/jnumed.118.221671

Prostate cancer is the second most frequently diagnosed cancer in men worldwide and is the sixth most diagnosed cancer in China (*1*). Early detection and accurate staging are critical for a favorable prognosis and clinical outcome (*2*). Prostate-specific membrane antigen (PSMA) is overexpressed in most cases of prostate cancer and is potentially associated with metastasis and progression of prostate cancer (*3*). Clinical studies have increasingly confirmed that PSMA is a valuable target for both the diagnosis and the treatment of prostate cancer (*4,5*). Radiolabeled urea derivatives, including ^{18}F-DCFBC (*6*), ^{18}F-DCFPyL (*7*), ^{68}Ga-PSMA-HBED-CC (*8*), ^{99m}Tc-MIP-1404 (*9*), ^{68}Ga/^{64}Cu-DKFZ-PSMA-617 (*10–12*), and ^{18}F-PSMA-1007 (*13,14*), have been reported to detect primary and metastatic prostate cancer lesions. PSMA PET imaging improves the detection rates for metastatic lesions in lymph nodes and bone, especially at low prostate-specific antigen levels (*14–20*). In addition, favorable imaging properties have also been demonstrated in nonprostate cancers (*21–25*).

Previous studies have shown that small-molecule PSMA radioligands had favorable clinical value in prostate cancer diagnosis, primary staging, prediction of risk stratification, monitoring of biochemical recurrence, and posttreatment evaluation (*26*). Compared with ^{68}Ga, the PET radionuclide ^{18}F exhibits several special advantages. The moderate half-life (109.7 min) and cyclotron preparation allow ^{18}F-labeled tracers to be synthesized with a high yield to be used in more patients and to be provided to other departments without on-site radiotracer production facilities. The increased positron yield (β^+ 97%) and shorter positron range (R_{ave} [average range] [β^+] = 0.69 mm) may potentially improve image quality (*27,28*). Al^{18}F has been developed as an ^{18}F-labeling technique that allows convenient ^{18}F labeling in less time and under milder conditions that can also be combined with a kit (*29–31*). Some ^{18}F-labeled PSMA ligands have been studied for preclinical evaluation, but none have been applied in clinical practice (*31,32*). Here, we report a novel Al^{18}F-labeled PSMA ligand and a pilot clinical study for further investigation.

Received Oct. 12, 2018; revision accepted Jan. 23, 2019.
For correspondence or reprints contact either of the following: Hua Zhu, Peking University Cancer Hospital and Institute, No. 52 Fu-Cheng Rd., Beijing, 100142, China.
E-mail: zhuhuananjing@163.com
Zhi Yang, Peking University Cancer Hospital and Institute, No. 52 Fu-Cheng Rd., Beijing, 100142, China.
E-mail: pekyz@163.com
*Contributed equally to this work.
Published online Feb. 22, 2019.
COPYRIGHT © 2019 by the Society of Nuclear Medicine and Molecular Imaging.

MATERIALS AND METHODS

General

All chemicals, reagents, and solvents were purchased commercially without further purification. The medium, fetal bovine serum, and penicillin–streptomycin solution were purchased from Gibco. ZJ-43 ((*S*)-2-(3-((*S*)-1-carboxy-3-methylbutyl)ureido), pentanedioic acid) was purchased from Tocris Bioscience. Sep-Pak Accell Plus QMA and Sep-Pak C18-Light cartridges were purchased from Waters, and an Acrodisc 25-mm syringe filter (0.2 μm) was purchased from Pall Corp. The no-carrier-added $Na^{18}F$ and ^{68}Ga-PSMA-617 were obtained from the Department of Nuclear Medicine, Peking University Cancer Hospital. The precursor PSMA-BCH (BCH is Beijing Cancer Hospital) was synthesized by China Peptides Co. The product was analyzed by radio–high-performance liquid chromatography (HPLC) (1200; Agilent) equipped with a γ-detector (Bioscan) with mobile phases of H_2O (A) and acetonitrile (B) mixed with 0.1% trifluoracetic acid. Radio-HPLC was performed using a linear A–B gradient (15%–60% B in 15 min) with a flow of 1 mL/min and 220-nm ultraviolet light. Small-animal PET was performed on a SuperArgus PET scanner (Sedecal). PET/CT scans were obtained on a Gemini TF scanner (Philips Medical Systems) with unenhanced low-dose CT.

Cell Culture and Tumor Models

PSMA-positive LNCaP and 22Rv1 and PSMA-negative PC-3 cell lines were provided by Stem Cell Bank, Chinese Academy of Sciences. LNCaP and 22Rv1 cells was cultured in RPMI-1640 medium, PC-3 cell lines were cultured in F12K medium, and both media were supplemented with 10% fetal bovine serum and 1% penicillin–streptomycin solution. Cells were incubated in a humidified incubator at 37°C and 5% CO_2.

22Rv1 cells (0.2 mL; 1×10^7 cells/mL) and PC-3 cells (0.2 mL; 1×10^7 cells/mL) were injected into the front leg of the male BALB/c nude mice, and LNCaP cells (0.1 mL; 4×10^7 cells/mL) and Matrigel (0.1 mL) were mixed and injected into the front leg of male NOD-SCID mice. When the tumors had grown to 5–10 mm in diameter, the mice underwent biodistribution and small-animal PET imaging studies. All animal studies were performed according to a protocol approved by the Animal Care and Use Committee of Peking University Cancer Hospital.

Radiolabeling and Quality Control

Radiosynthesis was based on a previous procedure, as shown in Figure 1 (*29*). $^{18}F^-$ was loaded onto a QMA cartridge and eluted by 0.5 mL of saline. No-carrier-added $^{18}F^-$ in saline (0.1 mL, 2.2–4.4 GBq), sodium acetate buffer (0.1 mL, 0.1 M, pH 4.0), and $AlCl_3$ (24 μL, 2 mM) in sodium acetate buffer (0.1 M, pH 4.0) were mixed and kept at room temperature for 5 min. Then, 20 μL of PSMA-BCH (4 mM, 80 nmol) were added and the mixture was heated at 110°C for 15 min. After cooling to room temperature, the reaction was diluted with 5 mL of H_2O and passed through a Sep-Pak C18-Light cartridge, which was pretreated with 10 mL of EtOH and 10 mL of H_2O. The Sep-Pak C18-Light cartridge was washed with H_2O (5 mL) and eluted with 0.6 mL of 80% EtOH to obtain the product, which was passed through a sterile filter membrane (0.2 μm) and diluted with saline for further studies. The radiochemical purity of $Al^{18}F$-PSMA-BCH was analyzed by radio-HPLC.

With a similar protocol, $Al^{19}F$-PSMA-BCH was synthesized and identified by matrix-assisted laser desorption/ionization-time-of-flight mass spectrometry. Details are shown in the supplemental materials (available at http://jnm.snmjournals.org).

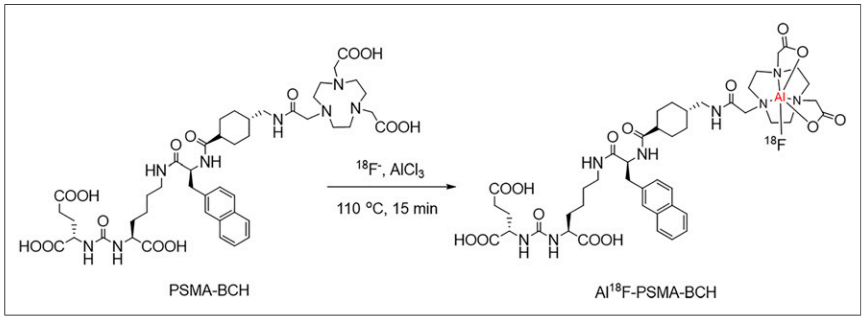

FIGURE 1. Preparation of $Al^{18}F$-PSMA-BCH.

Partition Coefficient

The partition coefficient was detected by adding 10 μL of $Al^{18}F$-PSMA-BCH (37 MBq, 13.56–15.34 GBq/μmol), 990 μL of phosphate-buffered saline (0.1 M, pH 7.4), and 1 mL of octanol to a tube. The mixture was vortexed for 3 min and centrifuged (3,000 rpm × 3 min). Then, 3 samples (100 μL) from each phase were removed and the radioactivity was measured by a γ-counter. The experiment was repeated 3 times. The partition coefficient was calculated as the average counts in octanol divided by the average counts in phosphate-buffered saline; the value was expressed as log P ± SD.

Stability

In vitro stability was studied by analyzing the radiochemical purity of $Al^{18}F$-PSMA-BCH by incubating in saline or in 5% human serum albumin for 2 h. In vivo stability was studied by analyzing the radiochemical purity of $Al^{18}F$-PSMA-BCH in blood and kidneys at 30 min after injection. The radiochemical purity was analyzed by radio-HPLC.

Cell Uptake

22Rv1 and PC-3 cells were plated on 24-well plates (1×10^5 cells per well) 24 h before the experiments. Half a milliliter of $Al^{18}F$-PSMA-BCH (74 KBq, 13.56–17.25 GBq/μmol) in fresh medium was added into each well. After 5, 30, 60, and 120 min, the medium was removed and the cells were washed with cold phosphate-buffered saline (1 mL × 2) and lysed by cold NaOH (1 M). The radioactivity was measured by a γ-counter. For blocking experiment, cells were coincubated with 1 μg of ZJ-43, a PSMA inhibitor. The result was expressed as percentage injected activity (%IA)/10^6 cells. This study was repeated 3 times.

The dissociation constant for $Al^{18}F$-PSMA-BCH was studied by adding different concentration of $Al^{18}F$-PSMA-BCH (13.56–17.25 GBq/μmol) to 22Rv1 cells in a 96-well plate. After incubation for 1 h, the medium was removed and the cells was washed twice with cold phosphate-buffered saline (0.1 mL × 2) and lysed by cold NaOH (1 M). The radioactivity was measured, and the dissociation constant was calculated with GraphPad Prism, version 5. The experiment was repeated 3 times.

Radiotoxicity

$Al^{18}F$-PSMA-BCH (0.2 mL, 13.2 GBq/μmol, 1.48 GBq/kg) was injected into 7 BALB/c male mice (25 g). For comparison, 7 mice were injected with 200 μL of saline. At 1, 2, 3, 4, and 7 d after injection, the mice were weighed and blood obtained from their orbit was analyzed by the Animal Laboratory of Peking University Health Science Center.

Biodistribution

Four mice bearing 22Rv1 and PC-3 tumors were injected with 200 μL of $Al^{18}F$-PSMA-BCH (0.74 MBq) via the tail vein, and 4

mice were coinjected with 50 μg of ZJ-43 for blocking. After 60 min, the mice were sacrificed, and the heart, liver, lung, kidney, spleen, stomach, bone, muscle, blood, gastrointestinal tract, and tumors were collected, weighed, and measured for radioactivity by the γ-counter. As a standard, 10 samples of 1% injected dose were taken from the injection and measured. The results are expressed as the percentage injected dose per gram (%ID/g).

Small-Animal PET Imaging

Mice bearing 22Rv1 and PC-3 xenograft tumors were intravenously injected with 200 μL of Al^{18}F-PSMA-BCH (14.8 MBq, 15.1 GBq/μmol) vail the tail vein with or without 50 μg of ZJ-43. The mice were anesthetized with 3% (v/v) isoflurane and underwent small-animal PET scans with continuous 1% (v/v) isoflurane. The images were obtained at 60 and 120 min after injection.

^{68}Ga-PSMA-617 (29.6 MBq, 14.8 GBq/μmol) and Al^{18}F-PSMA-BCH (14.8 MBq, 16.8 GBq/μmol) were injected into mice bearing LNCaP tumors, and small-animal PET imaging was performed at 90 min after injection.

Imaging was performed on a SuperArgus PET scanner using an 80-mm-diameter transaxial field of view, as well as ordered-subsets expectation maximization 3-dimensional reconstruction algorithms with attenuation and random corrections. Finally, the images were displayed by MMWKS Super Argus workstation software. The millicounts/s for regions of interest over tumor, kidney, and muscle were measured.

PET/CT Imaging and Analysis

The Al^{18}F-PSMA-BCH PET/CT imaging study was approved by the Ethics Committee of Beijing Cancer Hospital (approval 2017KT94), and all subjects signed an informed consent form. Considering the sink effect (*33*), 11 patients with biopsy-confirmed prostate cancer were included (age, 62.7 ± 13.3 y; range, 36–81 y; prostate-specific antigen level, 41.04 ± 41.43 ng/mL; range, 11.6–152.1 ng/mL; Gleason score, 7.4 ± 1.3; range, 6–9) (Table 1). Patients were intravenously injected with Al^{18}F-PSMA-BCH (2.0–3.2 MBq/kg, 16.21–18.90 GBq/μmol) and underwent PET/CT at 1 and 2 h after injection. Imaging was performed on a Gemini TF scanner (Philips Medical Systems) from head to middle of thigh. CT was performed using a voltage of 120 keV, a current of 100 mAs, a pitch of 0.8 mm, a single-turn tube rotation time of 0.5 s, and a scanning layer thickness of 3 mm. CT reconstruction used a standard method with a 512 × 512 matrix and a layer thickness of 3–5 mm. The PET images were acquired using a 3-dimensional model at 9–10 bed positions (90 s per bed position) and were reconstructed using ordered-subsets expectation maximization. Data from CT imaging were used to correct the PET images for attenuation. Whole-body CT and PET images were eventually obtained. The prostate cancer lesions and their SUV_{max} were determined by 2 experienced physicians, and data such as SUV_{mean}, average activity concentration (Bq/mm^3), and the volume of each organ at 1 and 2 h after injection were obtained to determine the organ biodistribution and to calculate the human organ dosimetry. Time-integrated activity coefficients were calculated individually (*34*), and human organ dosimetry was estimated using the OLINDA/EXM software (version 2.0; Hermes Medical Solutions AB) assuming no voiding of the urinary bladder until 2 h after injection as reported in the literature (*16*).

Statistical Analysis

All statistical analyses were completed using SPSS software (version 22.0; IBM Corp.). *P* values of less than 0.05 were considered statistically significant.

RESULTS

Synthesis of Al^{19}F-PSMA-BCH

Al^{19}F-PSMA-BCH was prepared and purified by HPLC with a mass spectrum of 965.412 ([M-F]$^+$) (Supplemental Fig. 1).

Radiolabeling

Al^{18}F-PSMA-BCH was manually prepared with a non–decay-corrected radiochemical yield of 32.2% ± 4.5%. The radiochemical purity was more than 99% as analyzed by radio-HPLC, with a retention time of 9.88 min (Supplemental Fig. 1). The specific activity was roughly calculated as 13.2–18.9 GBq/μmol ($n >$ 15). The injectate was colorless and transparent, and the quality control result is shown in Table 2.

Partition Coefficient and Stability

The log P value of Al^{18}F-PSMA-BCH was −2.76 ± 0.01, indicating that Al^{18}F-PSMA-BCH is highly hydrophilic.

TABLE 1
Patient Characteristics

No.	Age (y)	Weight (kg)	Injected dose (MBq)	PSA (ng/mL)	Gleason score
1	46	102	259.00	70.38	8
2	60	88	206.09	13.70	6
3	36	73	172.79	53.40	8
4	72	65	212.01	10.00	7
5	64	90	206.09	18.69	8
6	68	64	204.24	13.90	6
7	63	72	205.72	12.60	6
8	72	75	238.28	11.64	9
9	62	60	243.09	20.00	6
10	81	85	173.90	152.10	9
11	59	75	185.74	27.50	9

PSA = prostate-specific antigen.

TABLE 2
Quality Control of Al^{18}F-PSMA-BCH

Parameter	Result
Appearance	Colorless
Volume concentration	148 MBq/mL
pH	6.9–7.2
Radio–thin-layer chromatography	>99%
Radio-HPLC	>99%
Ethanol	<2%
Endotoxins	Pass
Sterility	Pass
Specific activity (GBq/μmol)	13.2–18.9

After incubation in saline (room temperature, 4 h) or 5% human serum albumin (37°C, 2 h), a single peak was observed on the HPLC chromatogram (Fig. 2A). Al^{18}F-PSMA-BCH was injected into mice, and the single peak that was observed on the HPLC chromatogram of Al^{18}F-PSMA-BCH was also consistently detected in blood and kidneys at 30 min after injection (Fig. 2B), indicating that Al^{18}F-PSMA-BCH was stable in vivo and in vitro within the time tested.

In Vitro Cellular Studies

Al^{18}F-PSMA-BCH showed significantly higher uptake in 22Rv1 cells than in PC-3 cells (Fig. 3A). The uptake in 22Rv1 cells was increased within 60 min (1.32 ± 0.10 %IA/10^6 cells), and the uptake was blocked to 0.61 ± 0.17 %IA/10^6 cells (−40.5%) by ZJ-43 at 60 min. The uptake in PC-3 cells was 0.61 ± 0.17 %IA/10^6 cells at 60 min and could not be blocked by ZJ-43. The dissociation constant for Al^{18}F-PSMA-BCH to PSMA in 22Rv1 cells was 2.90 ± 0.83 nM (Supplemental Fig. 2), indicating that the uptake of Al^{18}F-PSMA-BCH in 22Rv1 cells was PSMA-specific.

Radiotoxicity in Mice

No significant differences in weight or hematologic markers were observed between the mice injected with Al^{18}F-PSMA-BCH (1.48 GBq/kg) and those injected with saline within 1 wk of growing ($P > 0.05$, Supplemental Fig. 3). In addition, no lethal or chronic toxicity, hematologic effects, or biochemical effects were observed.

Ex Vivo Biodistribution

As shown in Figure 3B and Supplemental Table 1, 22Rv1 tumors showed the second highest uptake of Al^{18}F-PSMA-BCH (7.87 ± 2.37 %ID/g), whereas uptake in PC-3 tumors was much lower (0.54 ± 0.22 %ID/g). The uptake was significantly reduced in 22Rv1 tumors (0.46 ± 0.11 %ID/g, −94.2%, $P < 0.001$), as well as in the kidneys, spleen, and intestine, when coinjecting with 50 μg of ZJ-43. However, the uptake in PC-3 tumors was unaffected. The low uptake in nontarget organs caused high–PSMA-positive tumors to contrast with the 22Rv1/PC-3 ratio of 14.57 and the 22Rv1-to-kidney ratio of 0.56.

Small-Animal PET Imaging

Small-animal PET images of Al^{18}F-PSMA-BCH in mice bearing 22Rv1 and PC-3 tumors at 60 and 120 min after injection are shown in Figure 4A. The kidneys, bladder, and 22Rv1 tumors can be clearly visualized, whereas PC-3 tumor in the left armpit is almost invisible. The result is consistent with the biodistribution data. Similarly, radioactive accumulation in 22Rv1 tumors and kidneys was successfully blocked by 50 μg of ZJ-43.

In mice bearing LNCaP tumors, Al^{18}F-PSMA-BCH was highly accumulated in tumor, kidneys, and bladder (Fig. 4B). The LNCaP-to-muscle and LNCaP-to-kidney ratios were 64.5 and 1.18 at 90 min after injection, respectively. As control, ^{68}Ga-PSMA-617 small-animal PET was performed and showed similar results, with LNCaP-to-muscle and LNCaP-to-kidney ratios of 58 and 1.05, respectively. The LNCaP-to-muscle ratio was comparable, but the LNCaP-to-kidney ratio of Al^{18}F-PSMA-BCH was slightly higher ($P < 0.05$).

PET/CT Imaging and Analysis

During PET/CT imaging of 11 newly diagnosed prostate cancer patients, no adverse, clinically detectable pharmacologic effect or significant change in vital signs was observed. As shown in Supplemental Table 2 and Figure 5A, kidneys, submandibular glands, parotid glands, and lacrimal glands had intense radioactivity accumulation, with an SUV_{mean} of 16.26 ± 1.75, 10.77 ± 3.06, 7.10 ± 1.67, and 6.41 ± 2.32, respectively. The uptake of Al^{18}F-PSMA-BCH in these organs was significantly increased between 1 and 2 h after injection. SUV_{mean} was 19.52 ± 2.62 (+20.0%, $P < 0.001$), 13.22 ± 4.01 (+22.7%, $P = 0.041$), 9.06 ± 2.46 (+27.6%, $P = 0.002$), and 8.14 ± 2.96 (+27.0%, $P = 0.033$), respectively, at 2 h after injection.

Each of the 11 patients had at least 1 observable tumor lesion. The tumor burden is shown in Figures 5B and 5C. In total, 37 tumor lesions, including 17 lymph node metastases (in 6 patients) and 9 bone metastases (in 3 patients), were observed. Between 1 and 2 h after injection, the uptake was increased in 27 lesions, decreased in 9 lesions, and unchanged in 1 lesion. The mean SUV_{max} of all lesions increased from 10.60 to 14.11 (+33.1%, $P < 0.05$). Among 11 primary lesions, the SUV_{max} increased in 9 lesions, and the median

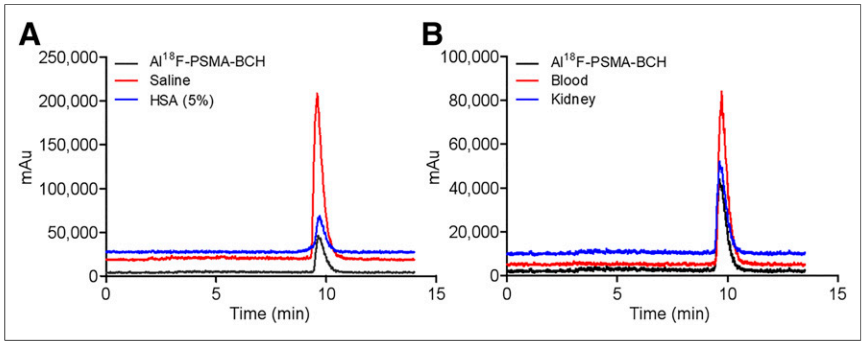

FIGURE 2. In vitro and in vivo stability of Al^{18}F-PSMA-BCH. (A) HPLC patterns of Al^{18}F-PSMA-BCH in saline (4 h) and 5% human serum albumin (HSA) (2 h). (B) HPLC patterns of Al^{18}F-PSMA-BCH in blood and kidneys for 30 min. Mobile phase was mixture of MeCN/0.1% trifluoracetic acid and H_2O/0.1% trifluoracetic acid: 5%–60% trifluoracetic acid in 0–15 min at flow rate of 1 mL/min. mAu = milli–absorbance units.

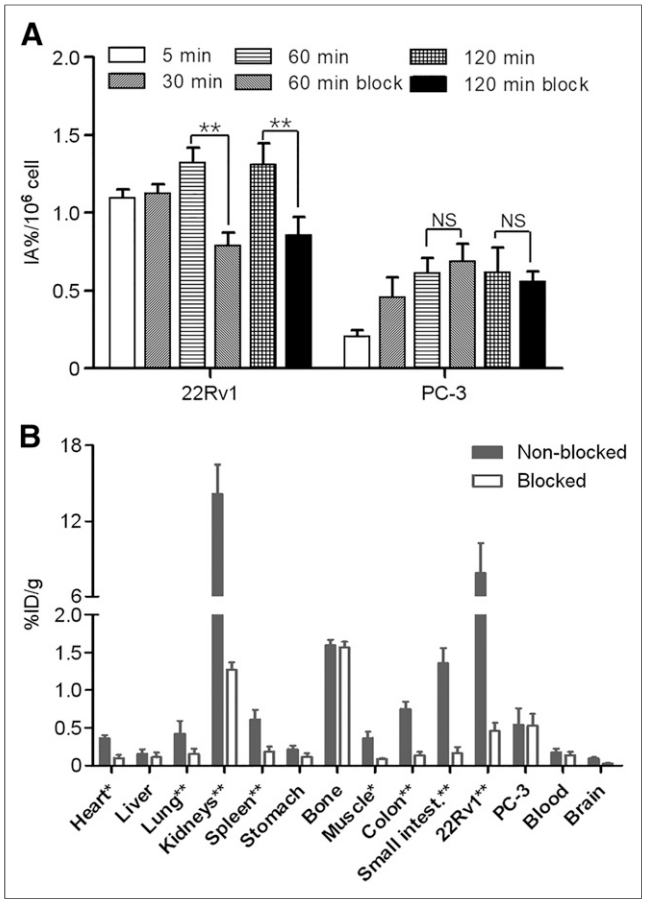

FIGURE 3. (A) Uptake of Al^{18}F-PSMA-BCH in 22Rv1 and PC-3 cells (n = 3). (B) Biodistribution in mice bearing 22Rv1 and PC-3 xenografted tumors. $^{**}P < 0.001$. $^{*}P < 0.05$. Block = ZJ-43; NS = not statistically significant.

SUV_{max} of 11 lesions increased from 16.38 (range, 3.60–34.13) to 21.68 (range, 3.34–46.79) between 1 and 2 h after injection. The SUV_{max} in 6 patients with a Gleason score of at least 8 (n = 6) was significantly higher than that in 5 patients with a Gleason score of less than 8 at 1 h after injection (20.23 vs. 11.75, P = 0.017) and 2 h after injection (27.02 vs. 15.27, P = 0.042). Among 17 lymph node metastases, the SUV_{max} increased in 14 lesions ($P < 0.001$), and the median SUV_{max} in 17 metastases increased from 9.26 (range, 3.09–24.28) to 12.77 (range, 2.72–38.89) between 1 and 2 h after injection. No significant difference in bone metastases was observed (P = 0.394), with a median SUV_{max} of 6.05 (range, 1.57–34.89) and 7.37 (range, 1.67–47.88) at 1 and 2 h, respectively, after injection. All 37 tumor lesions were visualized on the images at both 1 h and 2 h after injection.

As shown in Figures 6 and 7, the bladder, kidneys, liver, submandibular glands, lacrimal glands, and parotid glands were clearly visible at 1 and 2 h after injection. On the maximum-intensity projections of patients 7 and 9, the primary tumor lesions were clearly visualized. Intense uptake in the right fourth rib, right ilium, and right sciatic nerve is seen in Figure 6B. On the images of patient 3 (Fig. 7), intense uptake (SUV_{max} of 17.2 and 25.52 at 1 and 2 h after injection, respectively) was observed in the prostate gland, with invasion of the left seminal vesicle. Six lymph node metastases were clearly observed, with a median SUV_{max} of 12.34 (range, 7.60–24.28) and 18.88 (range, 9.78–38.89) at 1 and 2 h, respectively, after injection. One bone metastasis with a decreased SUV_{max} (2.15 vs. 1.90) was observed in the left fourth rib, but because of the low values, the bone metastasis in Figure 7 is not clear.

The calculated time-integrated activity coefficients (Supplemental Table 3) were used to estimate human organ radiation dosimetry. Organ radiation dosimetry and the effective dose are shown in Table 3. The kidneys were the most critical organ, with an absorbed dose of 0.135 ± 0.003 mGy/MBq, followed by the salivary glands (0.062 ± 0.014 mGy/MBq), spleen (0.033 ± 0.019 mGy/MBq), and liver (0.030 ± 0.007 mGy/MBq). The effective dose was 0.016 ± 0.002 mSv/MBq (range, 0.012–0.018 mSv/MBq). The effective dose that the 11 patients received was within the range of 2.10–4.03 mSv.

DISCUSSION

PSMA is an attractive target for the diagnosis and treatment of prostate cancer (*35*). PSMA probes labeled with ^{68}Ga and ^{18}F are reported to be successful in prostate cancer imaging. ^{18}F-labeled probes can meet more patients' needs with a single preparation because of the higher yield and longer half-life. The high resolution of ^{18}F and the convenience of the Al^{18}F chelating make Al^{18}F probes attractive (*31,36*). This study evaluated the biodistribution, radiation dosimetry, and preliminary efficacy of a novel tracer, Al^{18}F-PSMA-BCH. To the best of our knowledge, this is the first report of a human study on Al^{18}F PSMA tracers.

In this study, Al^{18}F-PSMA-BCH was manually prepared and characterized by Al^{19}F-PSMA-BCH, with a favorable nondecayed radiochemical yield (32.2% ± 4.5%, $n > 15$) within 30 min. The

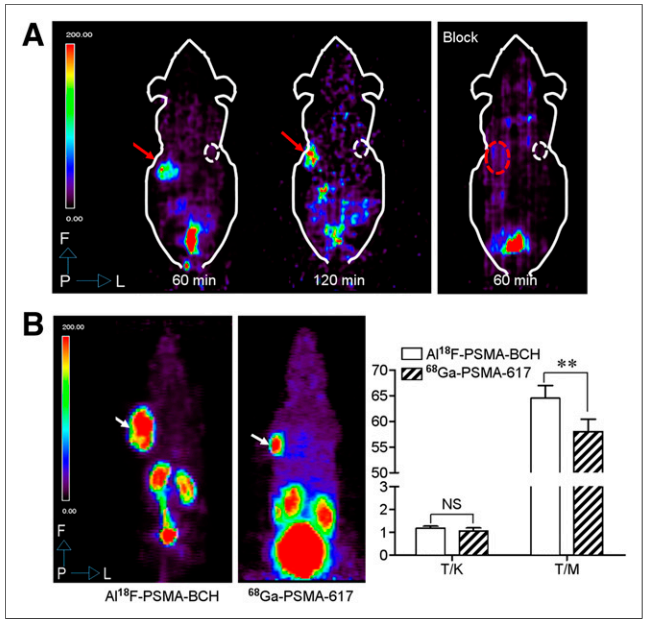

FIGURE 4. (A) Al^{18}F-PSMA-BCH PET images of mice bearing 22Rv1 and PC-3 tumors. (B) Maximum-intensity projections and tumor-to-nontarget ratios of Al^{18}F-PSMA-BCH and ^{68}Ga-PSMA-617 in mice bearing LNCaP tumors at 90 min after injection. Red arrows and circles indicate 22Rv1 tumors, white circles indicate PC-3 tumors, and white arrows indicate LNCaP tumors. $^{**}P < 0.001$. Block = coinjection with 50 μg of ZJ-43. NS = not statistically significant; T/K = tumor-to-kidney ratio; T/M = tumor-to-muscle ratio.

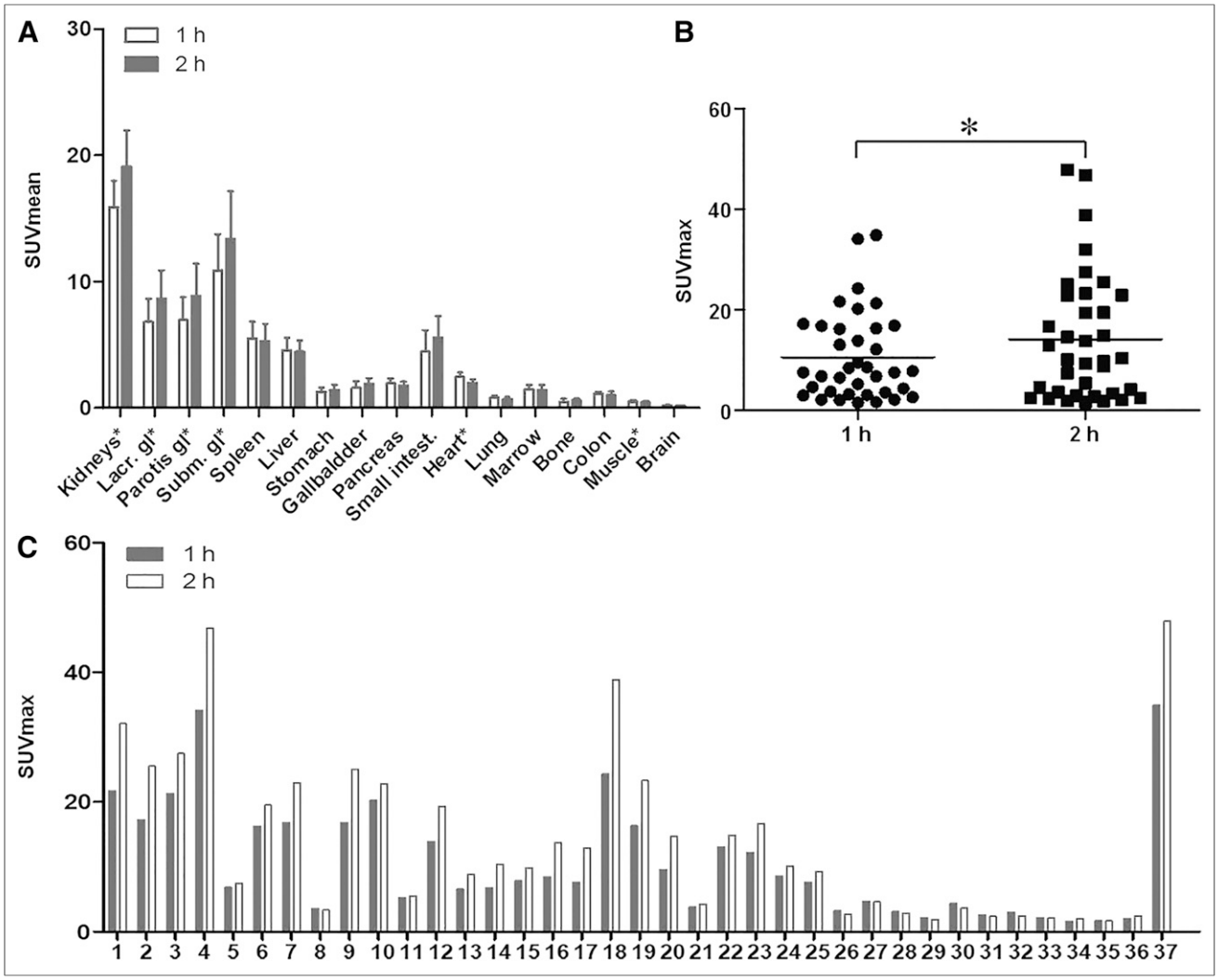

FIGURE 5. PET imaging data. (A) Biodistribution of Al^{18}F-PSMA-BCH in 11 newly diagnosed patients with prostate cancer. (B) Distribution of SUV_{max} in 37 tumor lesions. (C) SUV_{max} in all 37 tumor lesions at 1 and 2 h after injection (1–11 are primary tumors, 12–28 are lymph node metastases, and 29–37 are bone metastases). *$P < 0.05$.

reaction time was equivalent to that of ^{68}Ga-labeled tracers and far shorter than most ^{18}F-labeled radiotracers. The radioactivity of this radiotracer from each synthesis could reach 1.85 ± 0.37 GBq ($n > 5$) starting from approximately 7.4 GBq of $^{18}F^-$. This amount can meet the demand for at least 6 patients. In principle, automated synthesis of Al^{18}F-PSMA-BCH could easily be adapted for further studies, which may allow a higher radioactive dose. Quality control studies demonstrated that Al^{18}F-PSMA-BCH met the criteria of the 2015 edition of the Chinese pharmacopoeia and was qualified for clinical application.

No dissociated $^{18}F^-$ ion was detected in the stability study, indicating that Al^{18}F-PSMA-BCH was highly stable in vitro and in vivo. Though the bone uptake in mice bearing 22Rv1 and PC-3 tumors was higher (1.59 ± 0.07 %ID/g) than that in most nontarget organs, the uptake in humans was low (0.45 ± 0.23 at 1 h after injection and 0.54 ± 0.21 at 2 h after injection), and bone was nearly invisible on small-animal PET and PET/CT images. Bone metastases with an SUV_{max} of 1.57–34.89 could be detected, demonstrating that the bone uptake did not affect the image analysis and the detection of bone metastases.

The uptake of Al^{18}F-PSMA-BCH in cells and tumors was dependent on the PSMA level. The uptake of Al^{18}F-PSMA-BCH in 22Rv1 tumors and cells was higher than that in PC-3 tumors and cells and was blocked by excess ZJ-43, indicating that Al^{18}F-PSMA-BCH was specific to PSMA with high affinity. Al^{18}F-PSMA-BCH was highly accumulated in the kidneys and could be significantly blocked by ZJ-43 because of the high hydrophilicity of Al^{18}F-PSMA-BCH and the high PSMA level in the kidneys (*10,37,38*).

To evaluate the safety of Al^{18}F-PSMA-BCH at a high dose, single-dose radiotoxicity (1.48 GBq/kg) was examined in mice, and no lethal or chronic toxicity was observed. The injected dose of 2.05–4.05 MBq/kg for human studies was far below the tested dose and was considered safe for subjects.

To evaluate the detection capacity for tumors, the biodistribution in patients, and the absorbed dosimetry, Al^{18}F-PSMA-BCH PET/CT imaging was performed. According to the study of the sink effect by Filss et al., a high tumor burden may affect the uptake of PSMA radiotracers in organs (*33*). Therefore, patients with less than 10 tumor lesions and no multiple tumors were included in this study. Al^{18}F-PSMA-BCH showed high uptake in

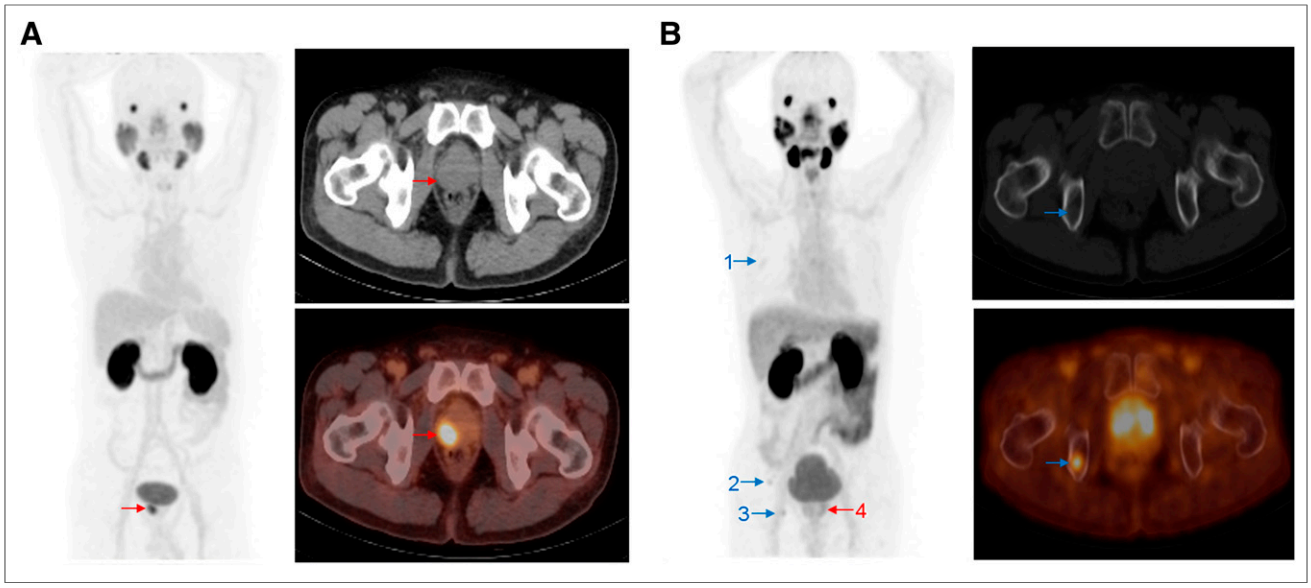

FIGURE 6. Maximum-intensity projections (left), CT images (top right), and PET/CT images (bottom right) of 2 patients at 1 h after injection. (A) In 63-y-old man with prostate-specific antigen level of 12.6 ng/mL and Gleason score of 3 + 3 = 6, CT and PET/CT images show primary tumor (SUV_{max}, 16.85). (B) In 62-y-old man with prostate-specific antigen level of 20 ng/mL and Gleason score of 3 + 3 = 6, CT and PET/CT images show 1 bone metastasis (metastasis 3: SUV_{max}, 4.37). Red arrows indicate primary tumors, and blue arrows indicate bone metastases.

PSMA-expressing organs, such as the kidneys, salivary glands, lacrimal glands, and parotid glands. The SUV_{max} and SUV_{mean} in these tissues and tumor lesions were significantly increased between 1 and 2 h after injection.

Among all 37 tumor lesions, the SUV_{max} was increased in 27 lesions, decreased in 9 lesions, and unchanged in 1 bone metastasis between 1 and 2 h after injection. In the 9 tumor lesions with a decreased SUV_{max}, the SUV_{max} was lower than 5 (2.15–4.69 at 1 h after injection and 1.90–4.59 at 2 h after injection). The slight decrease may be due to the reduced internalization rate of the radiotracer, as Afshar-Oromieh et al. reported for ^{68}Ga-HBED-CC (*39*), and the technique-related partial-volume effect, as reported by Wondergem et al. for ^{18}F-DCFPyL (*40*). Because all lesions visualized at 1 h after injection were also visible at 2 h after injection and the SUV_{max} and contrast were higher on the images of most patients at 2 h after injection, imaging at a later time point may be a better option. The SUV_{max} was significantly higher for patients with high-risk prostate cancer (Gleason score ≥ 8) than for patients with intermediate-risk prostate cancer—similar to the findings of a previous study on ^{68}Ga-PSMA-617 conducted by our group (*41*).

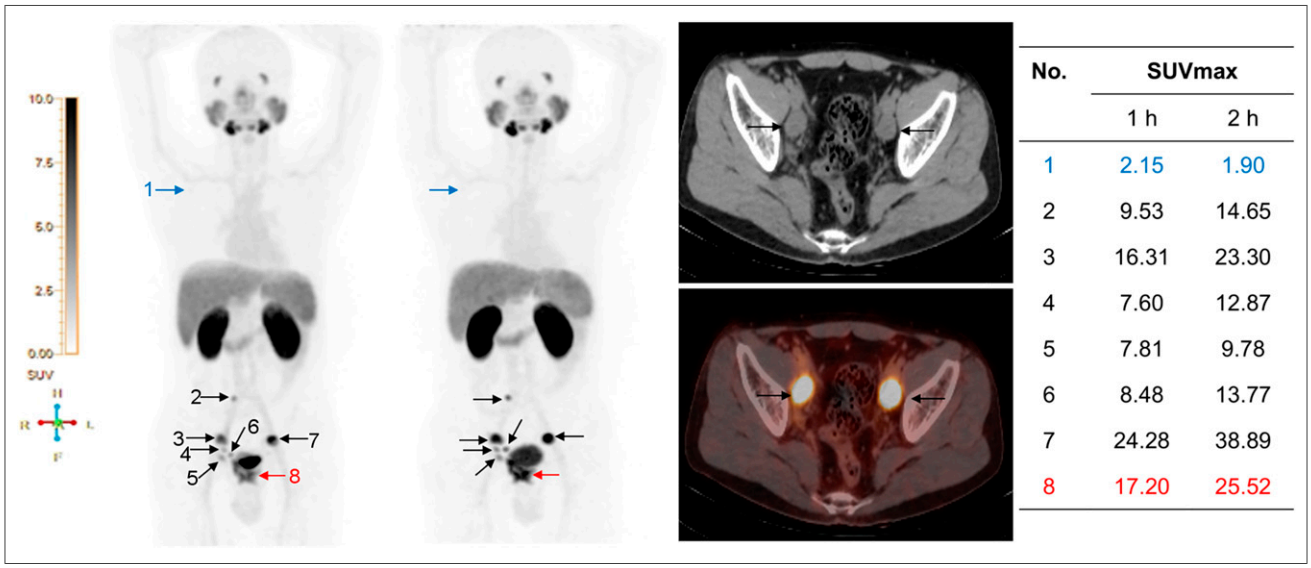

No.	SUVmax	
	1 h	2 h
1	2.15	1.90
2	9.53	14.65
3	16.31	23.30
4	7.60	12.87
5	7.81	9.78
6	8.48	13.77
7	24.28	38.89
8	17.20	25.52

FIGURE 7. In 36-y-old man with prostate-specific antigen level of 53.4 ng/mL and Gleason score of 4 + 4 = 8, images obtained 1 h after injection (left maximum-intensity projection) and 2 h after injection (right maximum-intensity projection, along with CT image [top] and PET/CT image [bottom]). Primary tumor (red arrows), 6 lymph node metastases (black arrows), and 1 bone metastasis (blue arrows) were visualized. CT and PET/CT images show 2 lymph node metastases (metastases 3 and 7).

TABLE 3
Human Organ Radiation Dosimetry Estimates for Al^{18}F-PSMA-BCH

Organ	Mean	SD	Minimum	Maximum
Adrenals	2.69E−02	5.29E−03	1.65E−02	3.48E−02
Brain	3.07E−03	5.28E−04	2.15E−03	3.78E−03
Esophagus	1.12E−02	9.69E−04	8.63E−03	1.19E−02
Eyes	5.90E−03	8.72E−04	3.83E−03	6.79E−03
Gallbladder wall	1.65E−02	2.42E−03	1.22E−02	2.01E−02
Left colon	1.74E−02	2.82E−03	1.29E−02	2.24E−02
Small intestine	2.18E−02	5.00E−03	1.54E−02	3.31E−02
Stomach wall	1.62E−02	2.42E−03	1.16E−02	1.99E−02
Right colon	1.41E−02	2.00E−03	1.04E−02	1.73E−02
Rectum	9.88E−03	1.52E−03	6.22E−03	1.15E−02
Heart wall	2.34E−02	1.91E−03	2.09E−02	2.76E−02
Kidneys	1.35E−01	3.12E−02	7.25E−02	1.89E−01
Liver	2.97E−02	7.31E−03	2.14E−02	4.25E−02
Lungs	1.78E−02	1.89E−03	1.42E−02	2.02E−02
Pancreas	1.55E−02	3.97E−03	9.39E−03	2.22E−02
Prostate	1.03E−02	1.74E−03	6.38E−03	1.21E−02
Salivary glands	6.22E−02	1.40E−02	4.16E−02	8.74E−02
Red marrow	8.61E−03	1.01E−03	6.33E−03	9.49E−03
Osteogenic cells	1.04E−02	1.36E−03	6.62E−03	1.18E−02
Spleen	3.27E−02	1.87E−02	1.01E−02	7.09E−02
Testes	7.06E−03	1.12E−03	4.39E−03	8.30E−03
Thymus	1.02E−02	7.455E−04	8.89E−03	1.12E−02
Thyroid	8.69E−03	1.30E−03	6.04E−03	1.06E−02
Urinary bladder wall	2.80E−02	7.64E−03	1.65E−02	3.60E−02
Total body	8.65E−03	1.68E−03	5.67E−03	1.00E−02
Effective dose (mSv/MBq)	0.0158	0.0019	0.0121	0.0180

Data are in mGy/MBq (n = 11).

The effective dose was calculated to be 0.016 ± 0.002 mSv/MBq, indicating that the effective dose of Al^{18}F-PSMA-BCH was within a reasonable range (*14*).

Although Al^{18}F-labeled PSMA radiotracers, ^{18}F-PSMA-11 (*31*), and Al^{18}F-NOTA-DUPA-Pep (*42*) have been reported, to the best of our knowledge, none of the Al^{18}F-labeled PSMA ligands have been reported for clinical evaluation. This pilot study reports initial experience with the dosimetry characteristics and tumor detectability of Al^{18}F-PSMA-BCH in prostate cancer. In our ongoing study, we will develop an automated synthesis method for Al^{18}F-PSMA-BCH and compare Al^{18}F-PSMA-BCH with other reported radiotracers. Regardless, the pilot study for Al^{18}F-PSMA-BCH demonstrated good imaging properties for prostate cancer. Considering the convenient labeling process, Al^{18}F-PSMA-BCH may be worthy of further clinical studies.

CONCLUSION

Qualified Al^{18}F-PSMA-BCH was obtained with good yield and with moderate specific activity within 30 min. Preclinical and clinical experiments demonstrated that Al^{18}F-PSMA-BCH can specifically accumulate in PSMA-expressing tumors with high binding affinity and good selectivity in the intact form. A clinical study of Al^{18}F-PSMA-BCH showed good detectability of tumor lesions with reasonable radiation exposure. Al^{18}F-PSMA-BCH has suitable properties and great potential for prostate cancer imaging.

DISCLOSURE

This work was financially supported by China Postdoctoral Science Foundation funded project 2018M631276; National Natural Science Foundation of China projects 81501519, 81571705, and 81671733; and Natural Science Foundation of Beijing Municipality project 7171002. No other potential conflict of interest relevant to this article was reported.

ACKNOWLEDGMENTS

We thank all the chemists, nurses, and technicians from the Department of Nuclear Medicine, Peking University Cancer Hospital, for their contributions in ^{18}F$^-$ and ^{68}Ga-DKFZ-PSMA-617 supply and PET/CT imaging.

KEY POINTS

QUESTION: Can Al^{18}F-labeled PSMA tracer be used for clinical PET/CT imaging of prostate cancer?

PERTINENT FINDINGS: A novel PSMA-based tracer Al^{18}F-PSMA-BCH was prepared with high stability and was PSMA-specific with high affinity. It can detect primary and metastatic tumor lesions with low radiation dosimetry.

IMPLICATIONS FOR PATIENT CARE: Al^{18}F-PSMA-BCH can be easily prepared to benefit more prostate cancer patients for PET/CT imaging.

REFERENCES

1. Siegel RL, Miller KD, Jemal A. Cancer statistics, 2017. *CA Cancer J Clin.* 2017;67:7–30.
2. Lai V, Khong PL. Updates on MR imaging and ^{18}F-FDG PET/CT imaging in nasopharyngeal carcinoma. *Oral Oncol.* 2014;50:539–548.
3. Violet JA, Hofman MS. Prostate-specific membrane antigen from diagnostic to therapeutic target: radionuclide therapy comes of age in prostate cancer. *BJU Int.* 2017;120:310–312.
4. Rowe SP, Drzezga A, Neumaier B, et al. Prostate-specific membrane antigen-targeted radiohalogenated PET and therapeutic agents for prostate cancer. *J Nucl Med.* 2016;57(suppl):90S–96S.
5. Afshar-Oromieh A, Babich JW, Kratochwil C, et al. The rise of PSMA ligands for diagnosis and therapy of prostate cancer. *J Nucl Med.* 2016;57(suppl):79S–89S.
6. Mease RC, Dusich CL, Foss CA, et al. N-[N-[(S)-1,3-Dicarboxypropyl]carbamoyl]-4-[^{18}F]fluorobenzyl-L-cysteine, [^{18}F]DCFBC: a new imaging probe for prostate cancer. *Clin Cancer Res.* 2008;14:3036–3043.
7. Chen Y, Pullambhatla M, Foss CA, et al. 2-(3-{1-carboxy-5-[(6-[^{18}F]fluoro-pyridine-3-carbonyl)-amino]-pentyl}-ureido)-pentanedioic acid, [^{18}F]DCFPyL, a PSMA-based PET imaging agent for prostate cancer. *Clin Cancer Res.* 2011;17:7645–7653.
8. Eder M, Schäfer M, Bauder-Wüst U, et al. ^{68}Ga-complex lipophilicity and the targeting property of a urea-based PSMA inhibitor for PET imaging. *Bioconjug Chem.* 2012;23:688–697.
9. Hillier SM, Maresca KP, Lu G, et al. ^{99m}Tc-labeled small-molecule inhibitors of prostate-specific membrane antigen for molecular imaging of prostate cancer. *J Nucl Med.* 2013;54:1369–1376.
10. Benešová M, Schäfer M, Bauder-Wüst U, et al. Preclinical evaluation of a tailor-made DOTA-conjugated PSMA inhibitor with optimized linker moiety for imaging and endoradiotherapy of prostate cancer. *J Nucl Med.* 2015;56:914–920.
11. Grubmüller B, Baum RP, Capasso E, et al. ^{64}Cu-PSMA-617 PET/CT imaging of prostate adenocarcinoma: first in-human studies. *Cancer Biother Radiopharm.* 2016;31:277–286.
12. Han XD, Liu C, Liu F, et al. ^{64}Cu-PSMA-617: A novel PSMA-targeted radiotracer for PET imaging in gastric adenocarcinoma xenografted mice model. *Oncotarget.* 2017;8:74159–74169.
13. Cardinale J, Schäfer M, Benešová M, et al. Preclinical evaluation of ^{18}F-PSMA-1007: a new PSMA-ligand for prostate cancer imaging. *J Nucl Med.* 2017;58:425–431.
14. Giesel FL, Hadaschik B, Cardinale J, et al. F-18 labelled PSMA-1007: biodistribution, radiation dosimetry and histopathological validation of tumor lesions in prostate cancer patients. *Eur J Nucl Med Mol Imaging.* 2017;44:678–688.
15. Schwenck J, Rempp H, Reischl G, et al. Comparison of ^{68}Ga-labelled PSMA-11 and ^{11}C-choline in the detection of prostate cancer metastases by PET/CT. *Eur J Nucl Med Mol Imaging.* 2017;44:92–101.
16. Green MA, Eitel JA, Fletcher J, et al. Estimation of radiation dosimetry for ^{68}Ga-HBED-CC (PSMA-11) in patients with suspected recurrence of prostate cancer. *Nucl Med Biol.* 2017;46:32–35.
17. Chan M, Hsiao E, Turner J. Cerebellar metastases from prostate cancer on ^{68}Ga-PSMA PET/CT. *Clin Nucl Med.* 2017;42:193–194.
18. Berliner C, Tienken M, Frenzel T, et al. Detection rate of PET/CT in patients with biochemical relapse of prostate cancer using [^{68}Ga]PSMA I&T and comparison with published data of [^{68}Ga]PSMA HBED-CC. *Eur J Nucl Med Mol Imaging.* 2017;44:670–677.
19. Barrio M, Fendler WP, Czernin J, Herrmann K. Prostate specific membrane antigen (PSMA) ligands for diagnosis and therapy of prostate cancer. *Expert Rev Mol Diagn.* 2016;16:1177–1188.
20. Giesel FL, Kesch C, Yun M, et al. ^{18}F-PSMA-1007 PET/CT detects micrometastases in a patient with biochemically recurrent prostate cancer. *Clin Genitourin Cancer.* 2017;15:e497–e499.
21. Rowe SP, Gorin MA, Hammers HJ, Pomper MG, Allaf ME, Javadi MS. Detection of ^{18}F-FDG PET/CT occult lesions with ^{18}F-DCFPyL PET/CT in a patient with metastatic renal cell carcinoma. *Clin Nucl Med.* 2016;41:83–85.
22. Sawicki LM, Buchbender C, Boos J, et al. Diagnostic potential of PET/CT using a ^{68}Ga-labelled prostate-specific membrane antigen ligand in whole-body staging of renal cell carcinoma: initial experience. *Eur J Nucl Med Mol Imaging.* 2017;44:102–107.
23. Sathekge M, Lengana T, Modiselle M, et al. ^{68}Ga-PSMA-HBED-CC PET imaging in breast carcinoma patients. *Eur J Nucl Med Mol Imaging.* 2017;44:689–694.
24. Noto B, Weckesser M, Buerke B, Pixberg M, Avramovic N. Gastrointestinal stromal tumor showing intense tracer uptake on PSMA PET/CT. *Clin Nucl Med.* 2017;42:200–202.
25. Siva S, Callahan J, Pryor D, Martin J, Lawrentschuk N, Hofman MS. Utility of ^{68}Ga prostate specific membrane antigen-positron emission tomography in diagnosis and response assessment of recurrent renal cell carcinoma. *J Med Imaging Radiat Oncol.* 2017;61:372–378.
26. Schwarzenboeck SM, Rauscher I, Bluemel C, et al. PSMA ligands for PET imaging of prostate cancer. *J Nucl Med.* 2017;58:1545–1552.
27. Dietlein M, Kobe C, Kuhnert G, et al. Comparison of [^{18}F]DCFPyL and [^{68}Ga]Ga-PSMA-HBED-CC for PSMA-PET imaging in patients with relapsed prostate cancer. *Mol Imaging Biol.* 2015;17:575–584.
28. Dietlein F, Kobe C, Neubauer S, et al. PSA-stratified performance of ^{18}F- and ^{68}Ga-PSMA PET in patients with biochemical recurrence of prostate cancer. *J Nucl Med.* 2017;58:947–952.
29. D'Souza CA, McBride WJ, Sharkey RM, Todaro LJ, Goldenberg DM. High-yielding aqueous ^{18}F-labeling of peptides via Al^{18}F chelation. *Bioconjug Chem.* 2011;22:1793–1803.
30. Shetty D, Choi SY, Jeong JM, et al. Stable aluminium fluoride chelates with triazacyclononane derivatives proved by x-ray crystallography and ^{18}F-labeling study. *Chem Commun (Camb).* 2011;47:9732–9734.
31. Boschi S, Lee JT, Beykan S, et al. Synthesis and preclinical evaluation of an Al^{18}F radiofluorinated GLU-UREA-LYS(AHX)-HBED-CC PSMA ligand. *Eur J Nucl Med Mol Imaging.* 2016;43:2122–2130.
32. Al-Momani E, Israel I, Samnick S. Validation of a [Al^{18}F]PSMA-11 preparation for clinical applications. *Appl Radiat Isot.* 2017;130:102–108.
33. Filss C, Heinzel A, Müller B, Vogg ATJ, Langen KJ, Mottaghy FM. Relevant tumor sink effect in prostate cancer patients receiving ^{177}Lu-PSMA-617 radioligand therapy. *Nuklearmedizin.* 2018;57:19–25.
34. Cho SY, Gage KL, Mease RC, et al. Biodistribution, tumor detection, and radiation dosimetry of ^{18}F-DCFBC, a low-molecular-weight inhibitor of prostate-specific membrane antigen, in patients with metastatic prostate cancer. *J Nucl Med.* 2012;53:1883–1891.
35. Fendler WP, Bluemel C, Czernin J, Herrmann K. PET imaging in prostate cancer, future trends: PSMA ligands. *Clin Transl Imaging.* 2016;4:467–472.
36. Machulla H-J, Al-Momani E. PSMA ligands for imaging prostate cancer: alternative labeling by complex formation with Al^{18}F^{2+}. *J Nucl Med.* 2017;58:2040–2041.
37. Harada N, Kimura H, Onoe S, et al. Synthesis and biologic evaluation of novel ^{18}F-labeled probes targeting prostate-specific membrane antigen for PET of prostate cancer. *J Nucl Med.* 2016;57:1978–1984.
38. Kelly J, Amor-Coarasa A, Nikolopoulou A, et al. Synthesis and pre-clinical evaluation of a new class of high-affinity ^{18}F-labeled PSMA ligands for detection of prostate cancer by PET imaging. *Eur J Nucl Med Mol Imaging.* 2017;44:647–661.
39. Afshar-Oromieh A, Sattler LP, Mier W, et al. The clinical impact of additional late PET/CT imaging with ^{68}Ga-PSMA-11 (HBED-CC) in the diagnosis of prostate cancer. *J Nucl Med.* 2017;58:750–755.
40. Wondergem M. Zant FMvd, Knol RJJ, Lazarenko S, Pruim J, Jong IJd. ^{18}F-DCFPyL PET/CT in the detection of prostate cancer at 60 and 120 minutes: detection rate, image quality, activity kinetics, and biodistribution. *J Nucl Med.* 2017;58:1797–1804.
41. Liu C, Liu T, Zhang N, et al. ^{68}Ga-PSMA-617 PET/CT: a promising new technique for predicting risk stratification and metastatic risk of prostate cancer patients. *Eur J Nucl Med Mol Imaging.* 2018;45:1852–1861.
42. Malik N, Zlatopolskiy B, Machulla H-J, Reske SN, Solbach C. One pot radiofluorination of a new potential PSMA ligand [Al^{18}F]NOTA-DUPA-Pep. *J Labelled Comp Radiopharm.* 2012;55:320–325.